scientific reports

Check for updates

OPEN

Relative DOA estimation method for UAV swarm based on phase difference information without fixed anchors

Yi Han[1], Jingjing Zhang[2,3]✉ & Jinglin Luo[4]

A key challenge for unmanned aerial vehicle (UAV) swarms is achieving inter-aircraft relative direction of arrival (DOA) estimation in global navigation satellite system (GNSS) denied environments without relying on fixed base stations. This paper proposes a Ultra-wide Bandwidth (UWB) based method where each UAV acts as both a transmitter and receiver, effectively functioning as a mobile base station. A theoretical framework for all-directional DOA estimation using a regular tetrahedral array is derived, resolving phase ambiguities via a genetic algorithm (GA) with phase difference information. Simulation results demonstrate that GA-UWB algorithm has a better performance than WP-UWB. When considering noise both in time difference and phase difference information, the algorithm proposed in this paper has a higher success rate.

Keywords UAV swarm, GNSS-denied environment, No base station, All-directional DOA Estimation

At present, the common methods of UAV swarms' mutual localization depend on GNSS technology. However, under the GNSS-denied environment, such as battlefield, tunnel and other environments, it is difficult to ensure that UAV can obtain the continuous and accurate positioning information. Compared with traditional signals, UWB signals have the advantages of low cost, insensitivity to channel fading, low power consumption, high security, and high positioning accuracy[1]. This technology has been applied to indoor positioning[2], deep wells and harsh environment portable equipment[3]. Currently, antenna arrays for UWB positioning, such as Uniform Circular Array (UCA)[4,5], are widely used in 2D direction estimation[6]. Most scholars carry out research on UWB indoor positioning algorithms based on basic positioning algorithms, such as time direction of arrival (TDoA) and angle of arrival (AoA) algorithm. Zhao et al.[7] approached the UWB TDoA localization from a system-level perspective, integrating sensor placement as a key component and conducting practical evaluation in real-world scenarios. Margiani et al.[8] presents an in-depth study and assessment of angle of arrival UWB measurements using a compact, low-power solution integrating a novel commercial module with phase difference of arrival estimation as integrated feature. Pan et al.[9] proposed a coplanar localization method for one-side-open areas, which is easy for deploying. In this method, the coordinates of the inside node can be estimated by the coplanar outside anchors that are attached to an outside window. Zhang et al.[10] presented a cost-effective UWB SL model utilizing the angle of arrival and double-sided two-way ranging. To improve localization accuracy, they proposed a self-localization algorithm based on constrained weighted least squares, integrating a weighted matrix derived from a measured noise model. Feng et al.[11] proposed one base station-based distance and angle positioning algorithm with extended Kalman filter in NLOS environment. Ge et al.[12] developed a single-anchor localization system which achieved 3D high-accuracy localization using time and wrapped phase measurements of UWB signals. Han et al.[13] introduced a methodology for refining ranging outcomes through a combination of UWB, inertial navigation and environmental adjustments to achieve high-precision spatial positioning. Krishnaveni et al.[14] come up with an incorporated positioning system in indoor by joining IMU and the UWB over the Unscented Kalman Filter and the Extended Kalman Filter to enhance the precision. Zhang et al.[15] advanced the UWB positioning system of the highway tunnel construction solution. Nevertheless, the implementation of these algorithms requires the installation of multiple fixed UWB base stations to ensure accurate positioning.

[1]School of Intelligent Manufacturing and Equipment, Shenzhen Institute of Information Technology, Shenzhen 518172, China. [2]School of Mechatronic Engineering and Automation, Foshan University, Foshan 528225, Guangdong, China. [3]Guangdong Provincial Key Laboratory of Industrial Intelligent Inspection Technology, Foshan University, Foshan, Guangdong, China. [4]Foshan Zhishi Technology Co., Ltd, Foshan, Guangdong, China. ✉email: jingjing@fosu.edu.cn

The deployment range of fixed UWB base stations is limited in large-scale environments, such as battlefields or wilderness areas. Hence, the scope of UAV swarms' tasks will be restricted.

To solve these problems, Luo et al.[16] designed a regular tetrahedral array (RTA) direction estimation sensor with UWB technology. A RTA consists with 4 UWB transceivers. These transceivers were installed on the vertices of a regular tetrahedron. As the distance between any two antennas in a RTA is greater than half of the signal wavelength, the phenomenon of phase ambiguity is existed during the process of estimating the source direction. Phase Ambiguity refers to the uncertainty in determining the true phase difference of a signal when the measured phase wraps around due to its periodic nature (typically modulo 2π). This occurs because phase measurements (e.g., in carrier-based systems like UWB) are cyclical, meaning a phase difference greater than π or less than $-\pi$ will "wrap" into the range $(-\pi, \pi]$. To solve the problem of phase ambiguity, a variable neighborhood search strategy using time difference information was proposed. However, the time difference measurement noises can be approximately 1600 times larger than phase difference measurement noises[17]. This can potentially lead to the initial solution provided by the above-mentioned method being significantly biased away from the correct solution, with the scanning range not covering the range of the correct solution, thus resulting in the inability to find the correct solution. Hence, it is important to reduce the noise impact caused by time difference information and use higher-precision phase difference information for localization calculations. Xu et al.[2] proposed a UWB-assisted positioning method using mobile nodes, optimizing phase ambiguity resolution in dynamic environments. Santos et al.[18] explored bearing-based estimation for distributed UAV swarms, validating the robustness of phase-difference information. This study provided theoretical validation for the phase difference information-based DOA estimation framework proposed in this paper. Li et al.[19] introduced deep learning for UWB phase ambiguity resolution, significantly improving performance under complex noise. Park et al.[20] systematically analyzed GA efficiency in sparse UWB array ambiguity resolution. This study directly supported the parameter design and performance validation of the GA-UWB algorithm.

In this paper, we derive the theoretical method of all-directional DOA estimation for regular tetrahedral array with phase difference signals only. Meanwhile, we will take use of GA to identify phase ambiguity integers with phase difference signals either. In conclusion, during the process of estimating the all-directional DoA of the signal source, we use phase difference information only which avoid the noises caused by time difference information.

Estimation of remote signal source for RTA using phase difference information

UWB transceiver can measure carrier phase more precisely than time-of-flight, the typical error value is less than 3°, which corresponds to 0.06 cm at f_c = 3.9936 GHz. Time difference measurements error is about 1600 times higher than phase difference measurements error[17]. For higher accuracy, we estimate the remote signal source with phase difference information only to avoid the impact of time difference measurement errors.

Spatial subarray decompose of RTA

As mentioned above, UCA can estimate the directional angle estimation in 2D space. To estimate the pitch angle, we can add a transceiver to a UCA and form a 3D antenna array. As equilateral triangle is the smallest unit in UCA, we can add a UWB transceiver to form a regular tetrahedral antenna array to estimate the signal source.

A RTA consists of four equilateral triangle subarrays, which can be treated as phased UCAs for solving 2D-AoA problems independently. Figure 1 depicts the decomposition of a tetrahedral and the spatial relationship between UCA subarrays and RTA.

In Fig. 1, $O_{\Delta BCD}, O_{\Delta ABD}, O_{\Delta ADC}, O_{\Delta ACB}$ are the circumcenter of $\Delta_{BCD}, \Delta_{ABD}, \Delta_{ADC}, \Delta_{ACB}$, which are shortened to $\Delta_1, \Delta_2, \Delta_3, \Delta_4$. ${}^{O}C = [O; \boldsymbol{x}, \boldsymbol{y}, \boldsymbol{z}]$ is the global coordinate system located at the original point O. ${}^{O_\Delta}C = [O_\Delta; \boldsymbol{e}_1, \boldsymbol{e}_2, \boldsymbol{e}_3]$ is the local coordinate system located at the centroid of a triangle. The transform matrix from ${}^{O_\Delta}C$ to ${}^{O}C$ is ${}^{O}_{O_\Delta}\boldsymbol{R} = [\boldsymbol{e}_1, \boldsymbol{e}_2, \boldsymbol{e}_3]$.

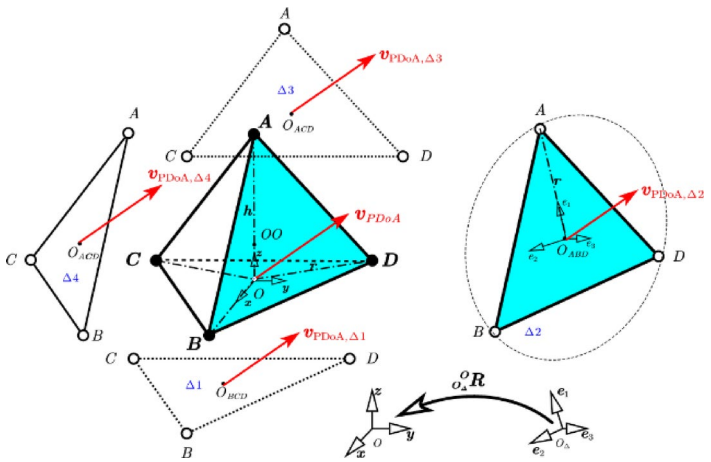

Fig. 1. Tetrahedral decomposition and spatial relationship[16].

We can estimate a signal direction vector (SDV) in each triangle. The SDVs estimated by four subarrays are recorded as $\boldsymbol{v}_{PDoA,\Delta_1} = \boldsymbol{v}_{PDoA,\Delta_2} = \boldsymbol{v}_{PDoA,\Delta_3} = \boldsymbol{v}_{PDoA,\Delta_4}$. In theory, the SDVs estimated by four subarrays are identical with a remote signal source hypothesis, which means $\boldsymbol{v}_{PDoA,\Delta_1} = \boldsymbol{v}_{PDoA,\Delta_2} = \boldsymbol{v}_{PDoA,\Delta_3} = \boldsymbol{v}_{PDoA,\Delta_4}$.

As shown in Fig. 1, we can design a tetrahedral source estimation sensor. Install a UWB signal transceiver at point A and install UWB signal receivers at points *B*, *C* and *D*. If we install the sensor on a UAV, the signal transceiver at point *A* can send its own signal to other UAVs. At the same time, according to the theory derived above, the source direction of other UAVs can be estimated through the phase difference signals received by the four points of *A*, *B*, *C*, *D*. In this way, each UAV equipped with a tetrahedral sensor can be used as a moving UWB base station to estimate all-directional DoA. This method can help the UAV swarm extending its applications as it is not necessary to install fixed UWB base stations.

Solve phased UCA

To avoid consuming computing resources in eigenvalues calculation, we solve the DoA estimation of any UCA subarray by Fourier analysis of the phase around the circular aperture[2,15]. Consider any UCA subarray which has *N* identical receivers and a remote signal source.

As shown in Fig. 2, the circular aperture is located at $(r, \pi/2, \varphi)$ and the remote source direction is located at (r, θ, φ). $\tilde{\phi}(\varphi)$ represents the continuous curve of actual phase difference $\phi(i,1)$. The period of $\tilde{\phi}(\varphi)$ is 2π. The purple ellipse $E_{S,\phi}$ is the projection of the aperture circle O_Δ on wave front plane *S*. $\tilde{\phi}(\varphi)\,\lambda/2\pi$ is the distance between any point on the aperture of circle O_Δ and its corresponding projection on $E_{S,\phi}$. The blue dashed line represents the intersection of $E_{S,\phi}$ and plane *S*. The normal vector of $E_{S,\phi}$ is $\boldsymbol{n}_S = \boldsymbol{v}_{PDoA,\Delta}$.

The phase of the electromagnetic field of an incident wave from (θ, φ) can be written as

$$\Phi(\varphi_i) = \frac{2\pi}{\lambda} r \sin\theta \cos(\varphi - \varphi_i) + \Phi_0 \tag{1}$$

Where the azimuth $\varphi \in [0, 2\pi)$ and the elevation $\theta \in [0, \pi)$. λ is the wavelength. Antennas are located counter-clockwise around the circular, and numbered 1 to 3. The azimuth position of antenna *i* is written as $\varphi_i = \frac{\pi(i-1)}{3}, i = 1, 2, 3$. Φ_0 is the initial phase of the incident wave and can be removed by the phase difference.

Taking antenna A_1 as a reference, the actual phase difference between antenna A_i and A_1 can be written as,

$$\phi(i,1) = \Phi(\varphi_i) - \Phi(\varphi_1) = \frac{4\pi r}{\lambda} \sin\theta \sin\left(\frac{\pi(i-1)}{M}\right) \sin\left(\varphi - \frac{\pi(i-1)}{M}\right) \tag{2}$$

The range of phase may exceed 2π as $r > \lambda/2$. Hence, the actual phase difference $\phi(i,1)$ is consisted of measured phase difference $\phi_0(i,1)$ and ambiguities $2\pi N_{i,1}$,

$$\phi(i,1) = \phi_0(i,1) + 2\pi N_{i,1}, \quad (\phi_0(i,1) \in (-\pi, \pi]) \tag{3}$$

The phase ambiguity integers $N_{i,1} \in \mathbb{Z}$ need to be solved. The first order Fourier series coefficient of $\phi(i,1)$ is[16],

$$\Psi 1 = \frac{2\pi}{M} \sum_{i=1}^{M} \phi(i,1) \exp\left(j \frac{2\pi(i-1)}{M}\right) \tag{4}$$

The elevation θ and azimuth φ can be derived as follows,

$$\theta = \sin^{-1}\left(\frac{\lambda}{2\pi^2 r} |\Psi 1|\right) \tag{5}$$

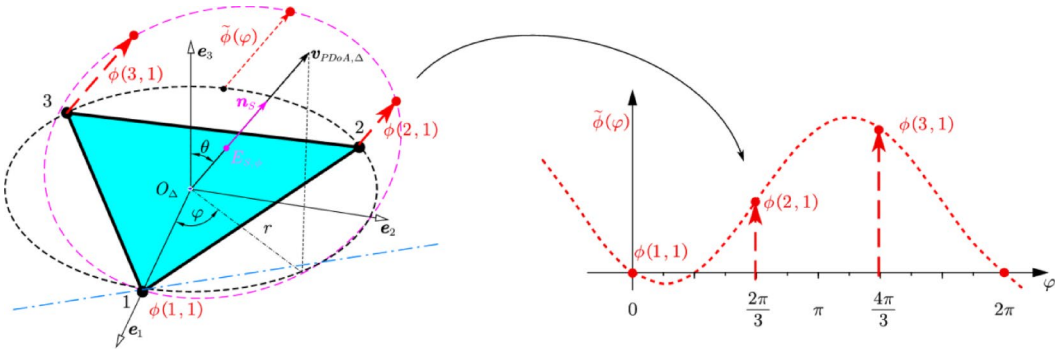

Fig. 2. The visualization of actual phase difference$\phi(i,1)$[16].

$$\varphi = \arg(\Psi 1) \tag{6}$$

,

Where $|\Psi 1|$ is the modulus of a complex number $\Psi 1$ and $\arg(\Psi 1)$ is the angle of $\Psi 1$.
Then we can obtain the SDV in coordinate ${}^{O_\Delta}C$[16],

$${}^{O_\Delta}\boldsymbol{v}_{PDoA} = [\cos\varphi\sin\theta, \sin\varphi\sin\theta, \cos\theta]^T \tag{7}$$

A direction vector in coordinate ${}^{O}C$ is derived by coordinate transform[16].

$${}^{O}\boldsymbol{v}_{PDoA} = {}^{O}_{O_\Delta}\boldsymbol{R}\,{}^{O_\Delta}\boldsymbol{v}_{PDoA} \tag{8}$$

Direction vector Estimation by genetic algorithm

Large aperture can improve the accuracy of AoA estimation. However, when the aperture radius is larger than $\lambda/2$, the phase ambiguity problem occurs. In previous work[16], we computed a coarse SDV estimation using time difference information initially. Then, we used the cost function based on geometric identical and variable neighborhood search strategy with time difference information to solve ambiguity resolution. As mentioned above, Ultra-wideband transceivers measured the information of carrier phases more accurately than the information of time of flight. The method of reducing noise impact caused by time difference information and using the higher-precision phase difference information for phase ambiguity is a worthwhile research direction. To solve this problem, this paper uses GA to solve the phase ambiguity integers with phase difference signal.

Geometric identical cost function

We proposed a cost function for ambiguity resolution based on the geometric identical of subarrays' SDVs. As Fig. 1 shows, SDVs estimated by four different subarrays are identical for a remote signal source. Without loss of generality, any two adjacent subarrays, such as, Δ_2 and Δ_3, they have common antennas *A* and *D*, and common reference antenna *A*. ${}^{O}\boldsymbol{v}_{PDoA,\Delta_2}$ and ${}^{O}\boldsymbol{v}_{PDoA,\Delta_3}$ are SDVs estimated in subarrays Δ_2 and Δ_3, respectively. The cost function consists of the noise between ${}^{O}\boldsymbol{v}_{PDoA,\Delta_2}$ and ${}^{O}\boldsymbol{v}_{PDoA,\Delta_3}$, which can be written as:

$$M23 = \left|1 - ({}^{\circ}v_{PDoA,\Delta 2})^{T\circ}v_{PDoA,\Delta 3}\right| \tag{9}$$

where the footnote 23 of M_{23} means subarray Δ_2 versus subarray Δ_3. Distinguishing from current cost function based on Fourier inverse transform or mapping tetrahedral volume[21], which estimating ambiguity integers firstly and then calculating DoA subsequently, unavoidable large rounding noises, our cost function is based on examining SDVs directly.

M_{23} is a scalar filed with 6 independent variables. Given phase difference information $\phi_0(B,A)$, $\phi_0(C,A)$, $\phi_0(D,A)$ as a priori knowledge. M_{23} can be reduced as discrete three dimensions, that is $M_{23}(N_{BA}, N_{CA}, N_{DA})$. Based on the above analysis, there are a total of 6 cost function values in an ultra-wideband regular tetrahedral array, which are related to the ambiguous integer array $N = \{N_{BA}, N_{CA}, N_{DA}, N_{CB}, N_{DB}\}$. The ambiguity resolution problem transforms into an optimization problem on discrete feasible set $N = \{N_{BA}, N_{CA}, N_{DA}, N_{CB}, N_{DB}\}$.

Ambiguity integers' calculations by genetic algorithm

In previous work, we used time difference information to obtain an initial ambiguous integer solution and scanned its neighbors to solve the phase ambiguity integers. But the measured noises of time difference information are huge. In this section, we will take use of GA to identify phase ambiguity integers with phase difference information only which avoid the noises caused by time difference information.

The specific steps of calculate ambiguity integers with phase difference information only by GA algorithm are as follows:

Step1: Determine the size of population *P*, generations *G*, crossover and mutation probabilities.

Step 2: Determine the parameters that will be optimized and encode these parameters with decimal integer.

Step 3: Determine the initial reference vector.

Step 4: Calculate the values of cost function *M* and the number of votes *D*.

Step 5: Propose the fitness function and calculate the fitness values of each individual.

Affected from phase difference measured noises, the number of votes may less than 6 even if P_i is the optimal individual. We propose a fitness function which consider the number of votes *D* and the maximum cost function value *M* that complies with ϵ comprehensively.

$$F = M \cdot 10^{-D}, (M = \max(M_{ij} < \varepsilon)) \tag{10}$$

where $\mathbf{F}$stands for the fitness function.

Step 6: Rank the population by fitness values and retain the best individual.

Step 7: Execute the step of crossover.

Step 8: Execute the step of mutation.

A new population has been created by combining the offspring from crossovers and mutated individuals. To avoid the premature convergence, we reinitialize 30% individuals with higher fitness values. If the fitness values of the best individual P_i satisfy the termination conditions in generation G, we will stop the parameter optimization. Otherwise, we will execute step 9.

Step 9: Repeat steps 4–8 with the opposite reference direction in step 3.

Step 10: Repeat step.

If the fitness values of the best individual satisfy the termination conditions in generation G, we will stop the parameter optimization. Otherwise, we will go back to step 3 and continue the following processes. The flow chart is shown in Fig. 3.

According to the geometric characteristics of a regular tetrahedral antenna, there are a certain number of wavelengths between any two antennas: $N \in [\ -N\_\max,\quad N\_\max\ ]$, $N\_\max = ceil(\sqrt{3}r \big/ \lambda + 0.5)$, where $\sqrt{3}r$ is the length of the regular tetrahedron and λ is the wavelength. To distinguish the algorithm proposed in this paper from the algorithm proposed in previous work, the algorithm mentioned in this paper will be referred to as "GA-UWB" in the following sections, and the algorithm introduced in the previous work will be abbreviated as "WP-UWB."

The time complexity of GA-UWB primarily depends on the population size P, generations G, and chromosome length L. As optimized three parameters are encoded with decimal integers, we define the chromosome length $L=3$. The overall complexity $O(P \cdot G \cdot L)_{\max} = P \times G \times L$. In contrast, WP-UWB relies on time difference -based initial guesses and local neighborhood scanning. Let K denote the number of candidate solutions explored per iteration. With N ambiguity integers to resolve, WP-UWB's complexity approximates $O(K \cdot N)$, where K grows exponentially with N in noisy scenarios.

GA-UWB employs global stochastic optimization, allowing it to escape local minima caused by time difference information noise. However, this requires larger P and G, increasing runtime. WP-UWB, while faster per iteration (linear in K), risks early convergence to suboptimal solutions due to time difference information noise sensitivity. In simulations, GA-UWB's runtime scales quadratically with G, whereas WP-UWB's runtime depends on the noise-induced expansion of K. Empirical tests show GA-UWB achieves stable convergence at SNR > 10 dB with $G = 50$, while WP-UWB fails consistently under high time difference information noise even with $K = 10^3$.This trade-off highlights GA-UWB's robustness in noisy environments at the cost of higher computational load, making it suitable for offline or high-performance UAV platforms.

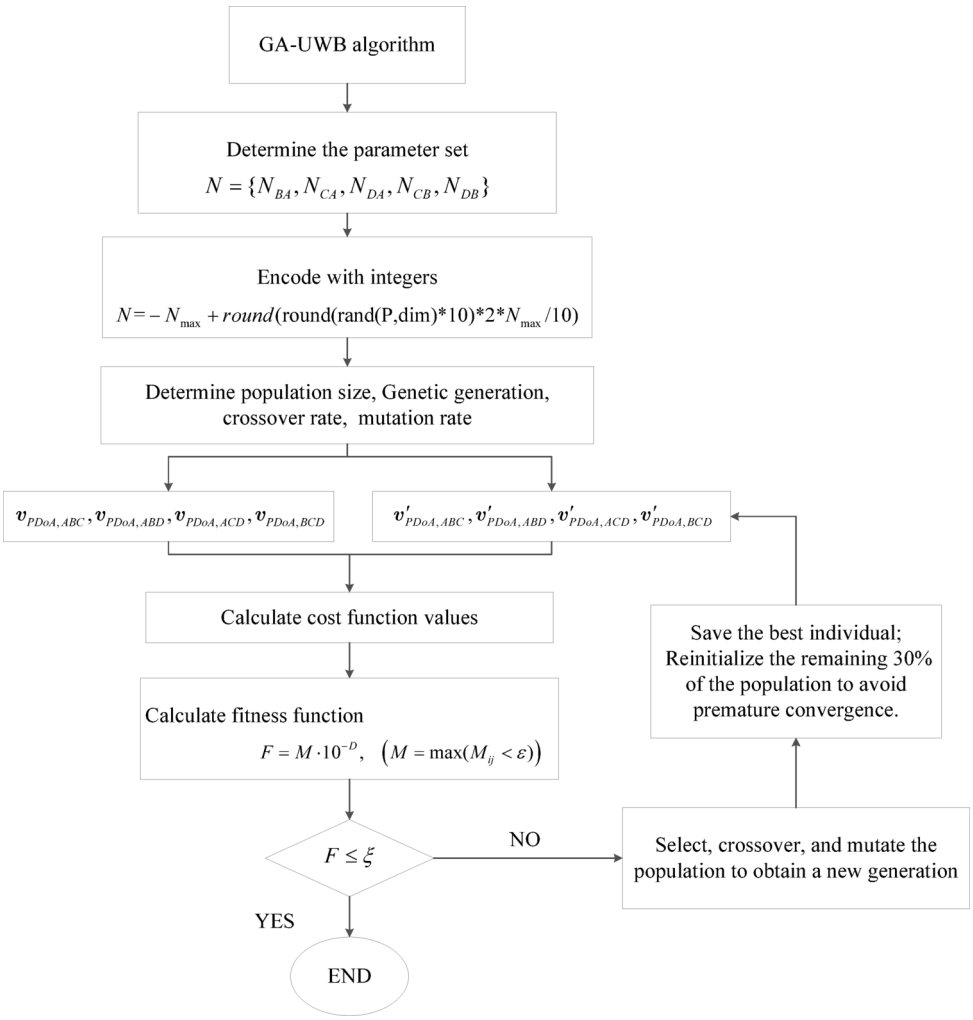

Fig. 3. Flow chart of GA-UWB algorithm.

Simulation

To demonstrate the effectiveness and performance of the proposed algorithm, simulation and numerical experiments were conducted. Using GA-UWB and WP-UWB algorithm, respectively, we predict the source direction for multiple location points and evaluate the two algorithms by calculation accuracy and success rate of source identification.

Assuming that the noise in time difference and phase difference measurements follows Gaussian white noise characteristics: $n_\tau \sim \mathcal{N}(0, \sigma_\tau)$ and $n_\phi \sim \mathcal{N}(0, \sigma_\phi)$, where σ_τ is the time difference measurement noise and σ_ϕ is the phase difference measurement noise. Meanwhile, the noises of each receiver are independent. For examining the accuracy of GA-UWB and WP-UWB, a series numerical experiments were conducted.

The radius of the regular tetrahedral antenna array's circumscribed sphere is about 12 cm, with the center point coordinates at (0, 0, 0). In order to meet the characteristics of a far-field signal source, 92 test points are uniformly selected on the surface of a sphere with a radius of 150 m, shown in Fig. 4.

Utilizing GA-UWB and WP-UWB separately, source direction estimation is conducted on these 92 points with the influence of different noise levels. Estimation error analysis is performed on the two sets of algorithms, as expressed in Eq. (5).

$$err = abs(1 - {v_{true}}^T \cdot v_{pre}) \times 100\% \tag{11}$$

Where v_{true} is the true far-field signal direction vector and v_{pre} is the estimated far-field signal direction vector. While $err \geqslant 0.0873$ (the angle between the true far-field signal direction vector and the estimated far-field signal direction vector is greater than 5 degrees), it is considered that the estimation vector is wrong.

In simulations, GA-UWB's runtime scales quadratically with population size *G*. However, the accuracy does not increase with the increase of *G*. Ultimately, we chose $G = 70$. Additionally, since the mutation probability should be small and the crossover probability should be large, the crossover probability $Pc = 0.75$ and mutation probability $Pm = 0.03$ were selected after a series of simulation analyses.

Taking the source direction with coordinates (0, 0, 150) as an example, the integer ambiguity is solved by using genetic algorithm.The curve of the fitness function value changing with the number of iterations during the optimization process is shown in Fig. 5. It can be seen that this algorithm has good convergence. When the calculation reaches the 12th generation, the fitness of the population reaches the minimum value, indicating that the optimization process has ended.

Influence of time difference measurement noises

Firstly, four random white noises are added to time difference signals received by the four antennas separately. The signal-to-noise ratio (SNR) ranges from $0dB$ to $50dB$ with $2dB$ increment and from $50dB$ to $100dB$ with $5dB$ increment, with a total of 36 groups. Each point undergoes 50 direction estimations at each SNR level. Figure 6 shows the variation of the average number of failure points as SNR level changes when using two algorithms for source direction estimation.

The result shows that as the time difference signal noise increases, WP-UWB algorithm fails to estimate the direction of each test point more frequently. This is because WP-UWB algorithm uses initial values determined from the noisy time difference signals when solving for the ambiguous integers.

Influence of phase difference measurement noise

Four random white noises are added to phase signals received by the four antennas separately. Figure 7 represents the variation of the average number of failure points as SNR level changes when using two algorithms for source direction estimation.

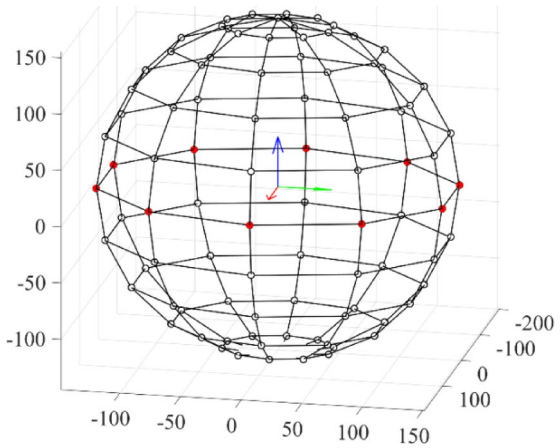

Fig. 4. Simulated test points.

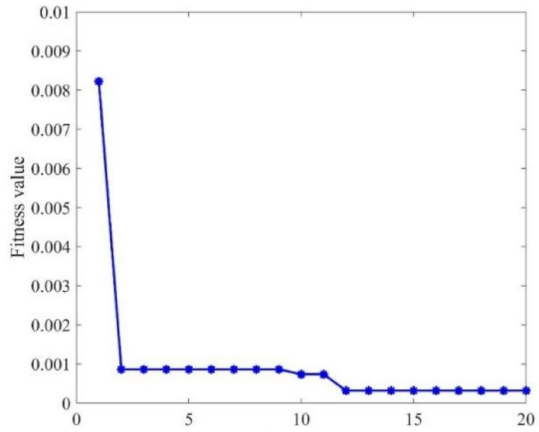

Fig. 5. Optimal fitness curves of genetic algorithm.

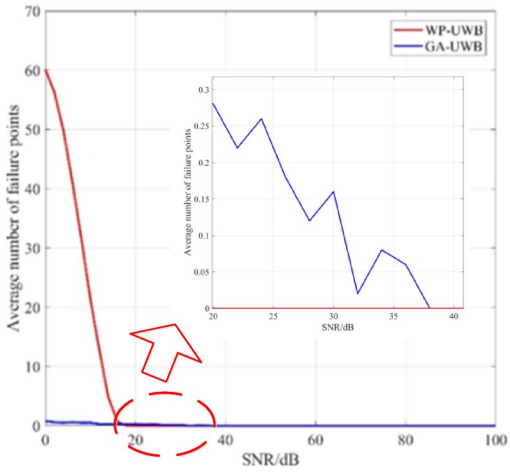

Fig. 6. Average number of failure points with time difference measurement noises.

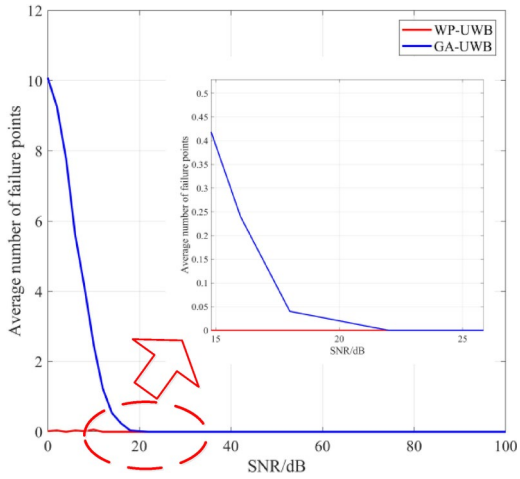

Fig. 7. Average number of failure points with phase difference measurement noises.

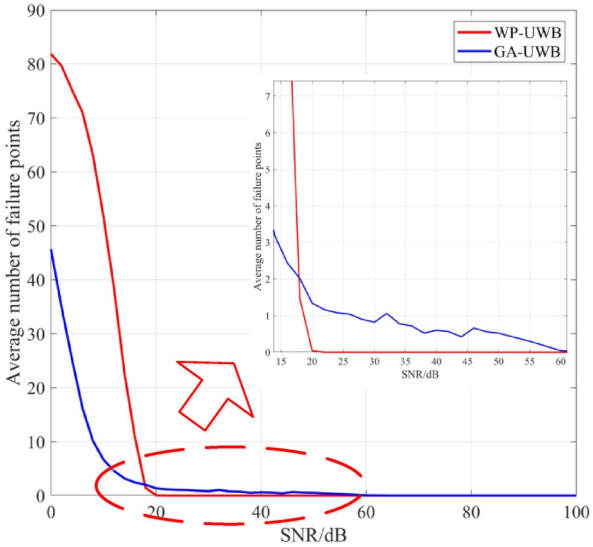

Fig. 8. Average number of failure points.

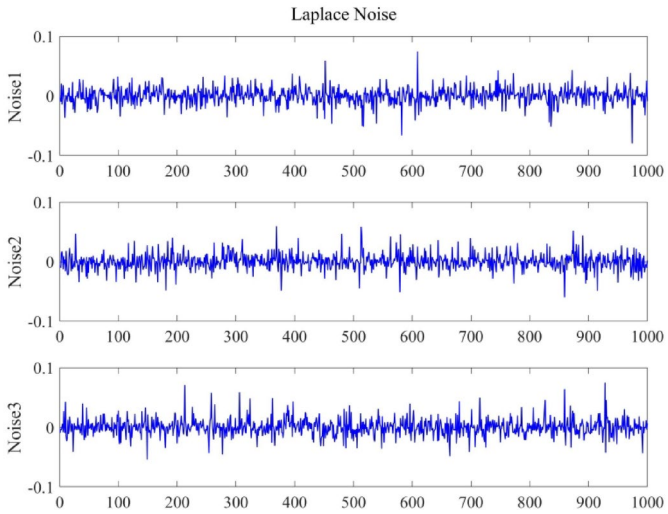

Fig. 9. Laplace noises.

The result shows that as the phase difference signal noise increases, GA-UWB algorithm fails to estimate the direction of each test point more frequently. When SNR exceeds 18dB, the influence of noises on signals become almost negligible.

Influence of time difference measurement noise and phase difference measurement noise

To simulate time difference and phase difference signals that are more representative of real conditions, series of random white noises are added to time difference signals and phase signals received by the four antennas separately. Figure 8 represents the variation of the average number of failure points.

The result shows that as the signal noise increases, both WP-UWB and GA-UWB algorithms experience a higher number of failures in estimating the direction vectors at various test points. However, when using the GA-UWB algorithm, it performs better than WP-UWB algorithm in both the number of estimation failures and the degree of angular deviation.

Influence of Laplace noise

Three conditions with Laplace noises have been analyzed in this paper. The noises shown in Fig. 9 will be added on time difference information separately, phase difference information separately, time difference and phase difference information synthetically.

Figure 10 shows the errors between estimated directions and true directions with 92 points by WP-UWB algorithm. Figure 11 shows the errors between estimated directions and true directions with 92 points by GA-

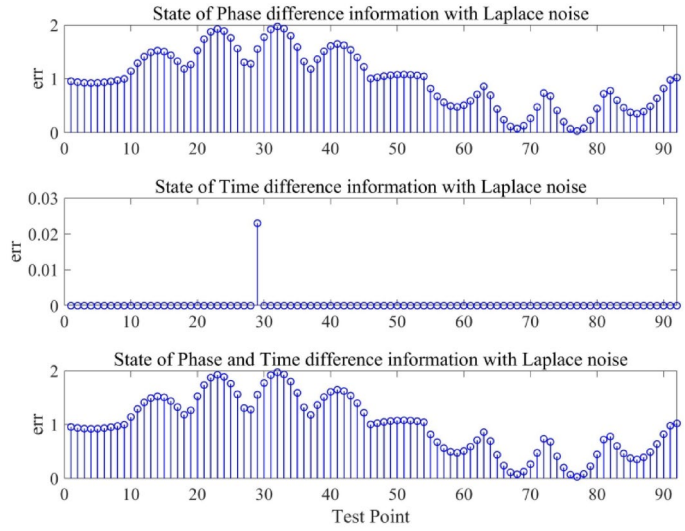

Fig. 10. Error between estimated direction and true direction with WP-UWB algorithm.

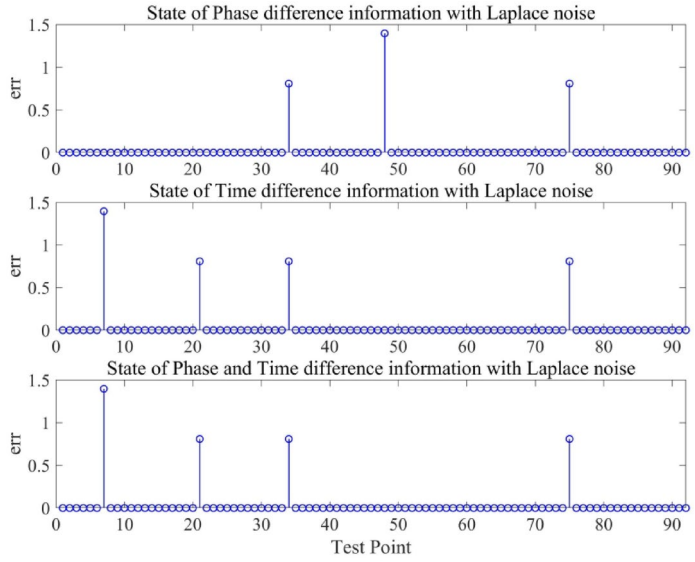

Fig. 11. Error between estimated direction and true direction with GA-UWB algorithm.

UWB algorithm. The results show that GA-UWB algorithm can obtain more estimated direction with the state of phase difference information with Laplace noise separately and the state of phase and time difference information with Laplace noise synthetically.

Influence of impulse noise

Three conditions with impulse noises have been analyzed in this paper. The noises shown in Fig. 12 will be added on time difference information separately, phase difference information separately, time difference and phase difference information synthetically.

Figure 13 shows the errors between estimated directions and true directions with 92 points by WP-UWB algorithm. Figure 14 shows the errors between estimated directions and true directions with 92 points by GA-UWB algorithm. The results show that GA-UWB algorithm can obtain more estimated direction with the state of phase difference information with impulse noise separately and the state of phase and time difference information with impulse noise synthetically.

Combined with Sects. "Influence of phase difference measurement noise", "Influence of time difference measurement noise and phase difference measurement noise", "Influence of Laplace noise" and "Influence of Impulse noise", the GA-UWB algorithm has a better performance to the WP-UWB algorithm in estimating direction vectors.

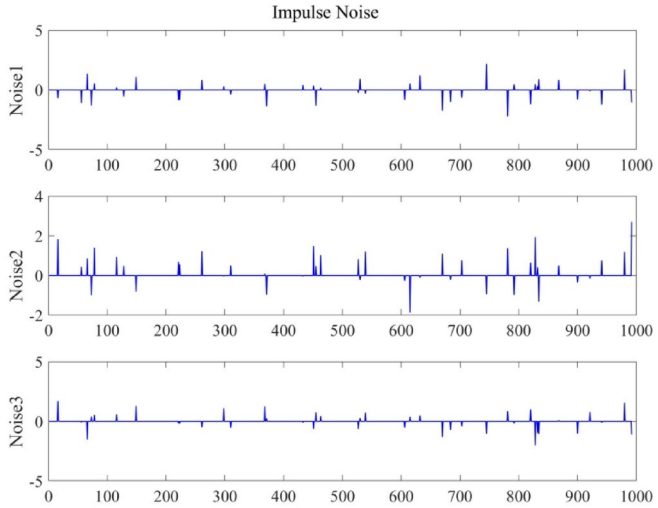

Fig. 12. Impulse noises.

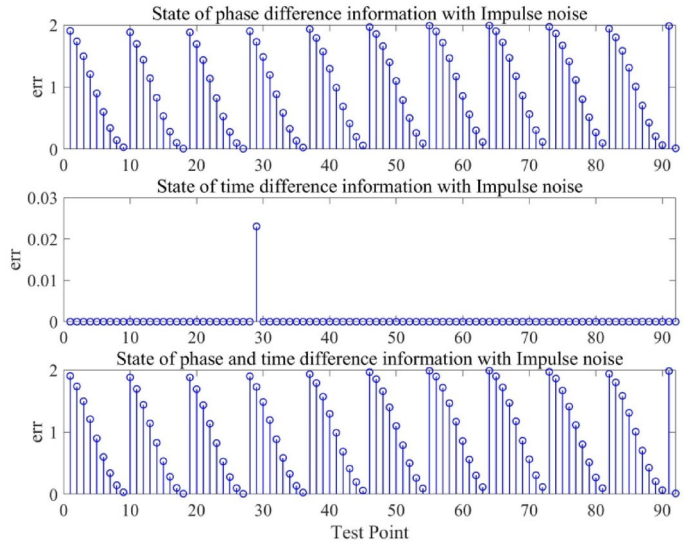

Fig. 13. Error between estimated direction and true direction with WP-UWB algorithm.

Conclusions

In this paper, we derived the remote source direction with a tetrahedral array by phase difference signals. In this process, we have taken use of phase difference signals only, which reduced the probability of source direction identification failure caused by time difference measurement error. When considering noise both in time difference and phase difference signals, the algorithm proposed in this paper achieves an average success rate of approximately 50.35% in estimating the source direction when SNR = 0dB. In contrast, the WP-UWB algorithm achieves only 11.02% success on average. As the SNR increases, the success rate of the algorithm proposed in this paper increases to an average of 92.76% when SNR = 10dB, while the WP-UWB success rate increases to 43.80% only.

The proposed GA-UWB algorithm significantly reduces failure rates and angular deviations compared to WP-UWB under noisy conditions, as demonstrated by simulations. However, these results are specific to the tested scenarios, where Gaussian white noise models were assumed for both time difference and phase difference measurements. While the algorithm shows robustness in these controlled environments, its performance may vary under non-Gaussian noise, correlated interference, or hardware calibration errors. Future work will validate the method in real-world conditions, including multipath propagation and dynamic swarm topologies. Despite these limitations, the GA-UWB framework provides a promising solution for UAV swarm localization in GNSS-denied settings.

Meanwhile, it is not necessary to install fixed UWB base stations in the process of UAV positioning, which extends the scope of the UAV swarm. Subsequently, according to the method proposed in this paper, we will

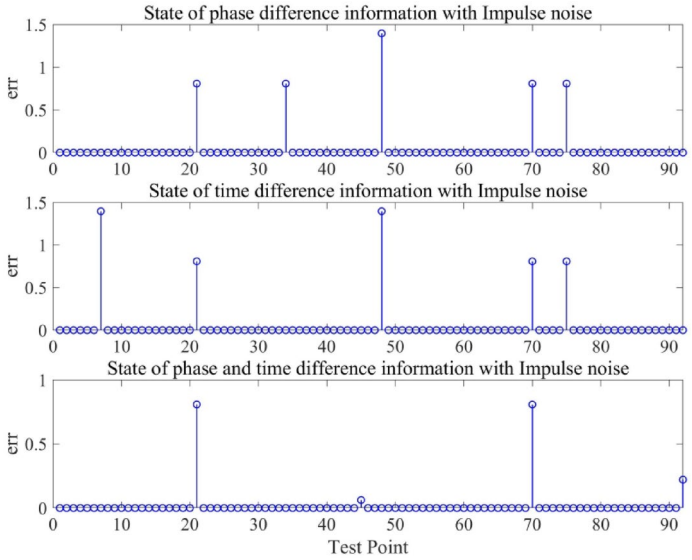

Fig. 14. Error between estimated direction and true direction with GA-UWB algorithm.

study the hardware and software development of mutual positioning sensor without fixed base stations between UAV swarms based on UWB technology, sensor networking, flight test of UAV swarm without fixed base stations independent of GNSS system, etc. to promote the practical development of UAV swarms.

Data availability

The data that support the findings of this study are available from the corresponding author upon reasonable request.

Received: 29 December 2024; Accepted: 8 April 2025
Published online: 24 April 2025

References

1. Ding, R., Qian, Z. & Wang, X. UWB positioning system based on joint TOA and DOA Estimation. *J. Electron. Inf. Technol.* **32**, 313–317 (2010).
2. Xu, J., Zhang, Y. & Han, Y. UWB indoor location method based on moving node auxiliary positioning. *J. Chin. Inert. Technol.* **31**, 141–147 (2023).
3. Chen, X., Yu, C. & Wen, Z. Application of UWB positioning technology in underground mine. *Coal Sci. Technol.* **46**, 187–189 (2018).
4. Zuo, L., Pan, J. & Shen, Z. Analytical algorithm for 3-D localization of a single source with uniform circular array. *IEEE Antennas Wirel. Propag. Lett.* **17**, 323–326 (2018).
5. Zuo, L. & Pan, J. Accurate 2-D AOA Estimation and ambiguity resolution for a single source under fixed uniform circular arrays. *Int. J. Antennas Propag.* **2017**, 1–6 (2017).
6. Dorsey, W. M., Mital, R. & Scholnik, D. P. IEEE,. Phase-only synthesis of omnidirectional patterns with multiple nulls from a uniform circular array. In *2016 IEEE Int. Symp. Antennas Propag. (APSURSI)*, Fajardo, PR, USA, 765–766 (2016).
7. Zhao, W., Goudar, A. & Schoellig, A. P. Ultra-wideband time difference of arrival indoor localization: from sensor placement to system evaluation. *ArXiv e-prints*. (2024).
8. Margiani, T., Cortesi, S., Keller, M., Vogt, Polonelli, C. T. & Magno, M. Angle of arrival and centimeter distance Estimation on a smart UWB sensor node. *IEEE T Instrum. Meas.* **2**, 1–10 (2023).
9. Pan, H. et al. An UWB-based indoor coplanar localization and anchor placement optimization method. *Neural Comput. Applic.* **34**, 16845–16860 (2022).
10. Zhang, D. et al. Accurate joint Estimation of position and orientation based on angle of arrival and Two-Way ranging of Ultra-Wideband technology. *Electronics-SWITZ* **14**, 429 (2025).
11. Feng, D. Q. et al. An adaptive IMU/UWB fusion method for NLOS indoor positioning and navigation. *IEEE Internet Things.* **10**, 11414–11428 (2023).
12. Ge, F. & Shen, Y. Single-Anchor Ultra-Wideband localization system using wrapped PDoA. *IEEE Mob. Comput.* **21**, 4609–4623 (2022).
13. Han, C., Xue, S., Long, L. & Xiao, X. Research on inertial navigation and environmental correction indoor Ultra-Wideband ranging and positioning methods. *SENSORS-BASEL* **24**, 261 (2024).
14. Krishnaveni, B. V., Reddy, K. S. & Reddy, P. R. Indoor tracking by adding IMU and UWB using unscented Kalman filter. *Wirel. Pers. Commun.* **123**, 3575–3596 (2022).
15. Zhang, H., Wang, X., Liu, Y. & Cai, L. Design and research of highway tunnel construction positioning system based on UWB. In: (eds Patnaik, S., Kountchev, R., Tai, Y. & Kountcheva, R.) 3D Imaging—Multidimensional Signal Processing and Deep Learning. Smart Innovation, Systems and Technologies, 349. Springer, Singapore. (2023).
16. Luo, J., Zhang, J., Yang, H. & Guan, Y. All-directional DOA Estimation for ultra-wideband regular tetrahedral array using wrapped PDoA. *Sensors* **22**, 1532 (2022).
17. APS014. Application note antenna delay calibration of DW1000-based products and systems. https://www.decawave.com
18. Santos, D. et al. Decentralized navigation systems for bearing-based position and velocity Estimation in tiered formations. *Int. J. Syst. Sci.* **53**, 504–525 (2022).

19. Li, Z., Wang, Q. & Chen, H. Robust UWB phase ambiguity resolution using deep learning for drone swarms. *IEEE Trans. Aerosp. Electron. Syst.* **58**, 3200–3215 (2022).
20. Park, S. & Kim, J. Genetic algorithm optimization for ambiguity resolution in sparse array UWB systems. *Sensors* **23**, 2567 (2023).
21. Xin, J. et al. Ambiguity resolution for passive 2-D source localization with a uniform circular array. *Sensors* **18**, 2650 (2018).

Author contributions

Conceptualization, Y.H., J.Z. and J.L.; methodology, Y.H., J.Z. and J.L.; software, J.Z.; validation, J.Z., Y.H. and J.L.; formal analysis, J.L.; investigation, Y.H.; resources, J.L.; data curation, J.L.; writing—original draft preparation, Y.H.; writing—review and editing, J.Z.; visualization, J.L.; supervision, Y.H.; project administration, J.Z.; funding acquisition, J.Z., J.L.; All authors have read and agreed to the published version of the manuscript.

Funding

The authors disclosed receipt of the following financial support for the research, authorship, and/or publication of this article: This work was partially supported by the National Natural Science Foundation of China (Grant No. 52005106).

Declarations

Competing interests

The authors declare no competing interests.

Additional information

Correspondence and requests for materials should be addressed to J.Z.

Reprints and permissions information is available at www.nature.com/reprints.

Publisher's note Springer Nature remains neutral with regard to jurisdictional claims in published maps and institutional affiliations.